Mon. Not. R. Astron. Soc. **373,** 1159–1172 (2006) doi:10.1111/j.1365-2966.2006.11091.x

Weak lensing by galaxies in groups and clusters – I. Theoretical expectations

Xiaohu Yang,[1,6]★ H. J. Mo,[2] Frank C. van den Bosch,[3] Y. P. Jing,[1,6] Simone M. Weinmann[4] and M. Meneghetti[5,7]

[1]*Shanghai Astronomical Observatory; the Partner Group of MPA, Nandan Road 80, Shanghai 200030, China*
[2]*Department of Astronomy, University of Massachusetts, Amherst, MA 01003-9305, USA*
[3]*Max-Planck Institute for Astronomy, Königstuhl 17, D-69117 Heidelberg, Germany*
[4]*Institute for Theoretical Physics, University of Zurich, CH-8057, Zurich, Switzerland*
[5]*Zentrum für Astronomie, ITA, Universität Heidelberg, Albert-Überle-Str. 2, D-69120 Heidelberg, Germany*
[6]*Joint Institute for Galaxy and Cosmology (JOINGC) of Shanghai Astronomical Observatory and University of Science and Technology of China*
[7]*INAF-Osservatorio Astronomico di Bologna, Via Ranzani 1, 40127, Bologna*

Accepted 2006 September 20. Received 2006 September 18; in original form 2006 July 24

ABSTRACT

Galaxy–galaxy lensing is rapidly becoming one of the most promising means to accurately measure the average relation between galaxy properties and halo mass. In order to obtain a signal of sufficient signal-to-noise ratio, one needs to stack many lens galaxies according to their property of interest, such as luminosity or stellar mass. Since such a stack consists of both central and satellite galaxies, which contribute very different lensing signals, the resulting shear measurements can be difficult to interpret. In the past, galaxy–galaxy lensing studies either have completely ignored this problem, have applied rough isolation criteria in an attempt to preferentially select 'central' galaxies, or have tried to model the contribution of satellites explicitly. However, if one is able to a priori split the galaxy population in central and satellite galaxies, one can measure their lensing signals separately. This not only allows a much cleaner measurement of the relation between halo mass and their galaxy populations, but also allows a direct measurement of the subhalo masses around satellite galaxies. In this paper, we use a realistic mock galaxy redshift survey to show that galaxy groups, properly selected from large galaxy surveys, can be used to accurately split the galaxy population in centrals and satellites. Stacking the resulting centrals according to their group mass, estimated from the total group luminosity, allows a remarkably accurate recovery of the masses and density profiles of their host haloes. In addition, stacking the corresponding satellite galaxies according to their projected distance from the group centre yields a lensing signal that can be used to accurate measure the masses of both subhaloes and host haloes. We conclude that an application of galaxy–galaxy lensing measurements to group catalogues extracted from large galaxy redshift surveys offers a unique opportunity to accurately constrain the galaxy–dark matter connection.

Key words: gravitational lensing – methods: statistical – galaxies: haloes – dark matter – large-scale structure of Universe.

1 INTRODUCTION

Understanding the connection between galaxies and dark matter haloes is a major challenge in modern astrophysics. From the perspective of cosmology, the galaxy–dark matter connection is required in order to translate observations of galaxy clustering in terms of the distribution of (dark) matter. From the perspective of galaxy formation, it reveals how halo mass impacts on the properties of the galaxies that form within them, and thus how the various physical processes that play a role in galaxy formation scale with halo mass. Consequently, a great amount of effort has been devoted to establishing the galaxy–halo connection, either through numerical simulations (e.g. Katz, Weinberg & Hernquist 1996; Fardal et al. 2001; Kay et al. 2002; Springel 2005; Springel et al. 2005), through semi-analytical modelling (e.g. White & Frenk 1991; Kauffmann, White & Guiderdoni 1993; Mo & Fukugita 1996; Mo, Mao & White 1998; Somerville & Primack 1999; Cole et al. 2000; Benson et al.

★E-mail: xhyang@shao.ac.cn

2002; van den Bosch 2002; Kauffmann et al. 2004; Croton et al. 2006), or via statistical approaches (e.g. Jing, Mo & Börner 1998; Seljak 2000; White 2001; Berlind & Weinberg 2002; van den Bosch, Yang & Mo 2003; Yang, Mo & van den Bosch 2003b; Cooray 2005, 2006; van den Bosch et al. 2005c; Zheng et al. 2005). However, neither of these methods provide a *direct* diagnostic of the galaxy–halo connection.

Direct measures of the dark matter haloes around galaxies come either from dynamical tracers or from gravitational lensing. Galaxy rotation curves and strong lensing, although extremely powerful, typically only probe the inner part of the dark matter halo, and are therefore not well suited to determine the total halo mass. The only dynamical tracers that probe the gravitational potential sufficiently far out to allow for an accurate mass estimate are satellite galaxies (Zaritsky & White 1994; McKay et al. 2002; Brainerd & Specian 2003; Prada et al. 2003; van den Bosch et al. 2004; Conroy et al. 2005). However, arguably the best method to directly probe the dark matter haloes around galaxies is galaxy–galaxy lensing, whereby the gravitational field of lensing galaxies induces small tangential shear distortions in the images of distant background galaxies (e.g. Natarajan & Kneib 1997). Unfortunately, since the weak-lensing signal around individual galaxies is too small to be detected, one can only infer ensemble-averaged properties: by combining the signal from a large number of lensing galaxies one obtains the galaxy-mass cross-correlation function, which can be used to infer the mass distribution around galaxies, but only in a statistical sense. Note, however, that a similar problem hampers the satellite-dynamics method, where the number of satellite galaxies of individual host galaxies is too small to allow for a reliable estimate of the halo mass, and ensemble averaging has to be used as well.

Since the galaxy–galaxy lensing signal is so weak, and one has to carefully correct for a number of observational effects, such as anisotropies in the point-spread function and shear induced by the camera optics, it took twelve years since the first attempt by Tyson et al. (1984) until the first detections of galaxy–galaxy lensing (Brainerd, Blandford & Smail 1996; dell'Antonio & Tyson 1996; Griffiths et al. 1996). In recent years, however, the progress has been enormous, largely due to the advent of deep galaxy surveys with large sky coverage (e.g. Fischer et al. 2000; McKay et al. 2001; Smith et al. 2001; Wilson et al. 2001; Hoekstra et al. 2003; Hoekstra, Yee & Gladders 2004; Sheldon et al. 2004; Hoekstra et al. 2005; Parker et al. 2005; Kleinheinrich et al. 2006; Mandelbaum et al. 2006a,b).

The fact that galaxy–galaxy lensing only yields ensemble averaged properties complicates the interpretation. Since galaxies with different luminosities and morphologies are expected to reside in haloes of different masses, the ensemble averages are complicated sums over large ranges in halo mass. Unless one has a prior knowledge of the relation between galaxy properties and halo mass, an unbiased interpretation of the measurements is basically impossible. For example, in the past most studies have used the observed lensing signal only to constrain the normalization of an *assumed* relation between galaxy luminosity, L, and halo mass, M (e.g. Fischer et al. 2000; Smith et al. 2001; Wilson et al. 2001; Hoekstra et al. 2003). When redshift information regarding the lenses and/or sources is available, one can somewhat improve the constraints. For example, Hudson et al. (1998) were able to simultaneously constrain the normalization and the slope of the L–M relation, due to the fact that they had photometric redshifts available for both their lenses and their sources. Nevertheless, their results clearly depend on the assumed functional form (a power-law) of the L–M relation.

Therefore, one of the ultimate goals in galaxy–galaxy lensing is to be able to measure the lensing signals for galaxies with different intrinsic properties. This requires not only a very large sample of galaxies (both lenses and sources), but also redshifts for the lensing galaxies, in order to be able to (i) convert angular sizes into physical sizes, (ii) compute the luminosities of the lenses and (iii) reduce uncertainties in the geometry of the lens-source system. The Sloan Digital Sky Survey (SDSS) has proven to be ideally suited to make progress along such a direction, and several measurements of the galaxy–galaxy lensing signal as function of galaxy luminosity and morphological type have already been made (e.g. McKay et al. 2001; Sheldon et al. 2004; Mandelbaum et al. 2006a).

There is one additional problem that complicates the interpretation of these lensing signals, namely the distinction between 'central' galaxies, which reside at the centre of a dark matter halo, and 'satellite' galaxies, which are located on an orbit around a central galaxy. In the current paradigm, these satellite galaxies are thought to be associated with dark matter subhaloes, which are haloes that reside and orbit within a larger virialized dark matter halo. The idea that satellite galaxies are related to the population of dark matter subhaloes is consistent with both observations and numerical simulations (e.g. Kravtsov et al. 2004; Natarajan & Springel 2004; Vale & Ostriker 2004, 2006; Kang et al. 2005; Conroy, Wechsler & Kravtsov 2006; Natarajan, De Lucia & Springel 2006). The lensing signal around a satellite galaxy does reflect not only the mass distribution of the dark matter subhalo in which it is located, but also that of the larger halo that hosts the subhalo (hereafter host halo). Thus, one expects the lensing signal from a satellite galaxy to be very different from that of a central galaxy (e.g. appendix B in Yang et al. 2003a). In addition, the lensing signal from a satellite galaxy depends not only on the masses of the subhalo and host halo, but also on the geometrical orientation of these two entities with respect to each other.

Since a galaxy of a given luminosity and/or morphological type can be either a central galaxy or a satellite galaxy, even the lensing signal from a sample of lensing galaxies with a narrow range in luminosities and morphological types can be difficult to interpret. In the past, galaxy–galaxy lensing studies either have completely ignored this problem (e.g. McKay et al. 2001; Hoekstra et al. 2003, 2004), have applied rough isolation criteria in an attempt to preferentially select 'central' galaxies (e.g. Hoekstra et al. 2005; Mandelbaum et al. 2006b), or have modelled the contribution of satellites explicitly, using either semi-analytical models for galaxy formation (Guzik & Seljak 2001; Yang et al. 2003a) or a model for the halo occupation statistics (Guzik & Seljak 2002; Mandelbaum et al. 2005b, 2006a). None of these approaches have taken into account the weak-lensing signals around satellite galaxies at different halo-centric distances.

In this paper, we demonstrate that it is actually possible to measure the lensing signal around satellite galaxies at different projected halo-centric distances, provided that a well-defined sample of galaxy groups and clusters is available to represent galaxy distribution in dark matter haloes. This not only allows a much cleaner measurement of the relation between halo mass and their galaxy populations, but also allows a direct measurement of the subhalo masses around satellite galaxies. Using realistic mock galaxy catalogues we show that the halo-based group finder, recently developed by Yang et al. (2005a), allows an accurate identification of central and satellite galaxies, and that their corresponding lensing signals allow an accurate recovery of their mean host and subhalo masses, respectively. Note also that in order to perform such a measurement, a large spectroscopic sample is needed to group lensing galaxies according to their common haloes. Currently, the largest sample of this

kind is from the SDSS. With about one-third of the eventual SDSS, significant galaxy–galaxy lensing signals have been detected separately for three (seven) subsamples in galaxy luminosity and colour (e.g. Sheldon et al. 2004; Mandelbaum et al. 2006a). This suggests that the present SDSS data may already be able to probe the lensing signals around galaxies in broad bins of halo mass and halo-centric distances. With the completion of the SDSS, and with future deeper imaging surveys in the same part of the sky as the SDSS, we anticipate that the effects we are considering here can be studied. In a forthcoming paper, we will construct shear maps from realistic mock catalogues taking into account observational effects to test the feasibility of the method we are proposing here.

This paper is organized as follows. In Section 2 we give a detailed description of the weak-lensing signal produced by host haloes and subhaloes, separately. In Section 3 we use realistic mock catalogues constructed from *N*-body simulations to demonstrate how to split the galaxy population in central and satellite galaxies, and how their lensing signals allow a measurement of their corresponding host and subhalo masses, respectively. Our conclusions are summarized in Section 4.

2 LENSING BY HALOES AND SUBHALOES

Galaxy–galaxy lensing measures the profiles of the tangential shear, $\gamma_{\rm t}(R)$, azimuthally averaged over a thin annulus of projected radius R around a set of lens galaxies. This observable quantity is related to the mean projected surface mass density within the aperture radius R according to

$$\gamma_{\rm t}(R)\Sigma_{\rm crit} = \Sigma(\leqslant R) - \Sigma(R) \equiv \Delta\Sigma(R). \tag{1}$$

Here $\Sigma(\leqslant R)$ is the mean surface density within R, $\Sigma(R)$ is the azimuthally averaged surface density at R and

$$\Sigma_{\rm crit} = \frac{c^2}{4\pi G}\frac{D_{\rm s}}{D_{\rm l}D_{\rm ls}} \tag{2}$$

is the critical density, which is determined by the geometry of the lens-source system (Miralda-Escudé 1991; see Schneider 2005 for a detailed review). In the above equation, $D_{\rm l}$, $D_{\rm s}$ and $D_{\rm ls}$ are the angular diameter distances to the lens, to the source and between the lens and the source, respectively. Since a uniform mass sheet, such as the mean density of the universe, does not contribute to $\Delta\Sigma$, it basically measures the *excess* surface density (hereafter ESD).

The mean ESD around a galaxy is specified by the line-of-sight projection of the galaxy-matter cross-correlation function, $\xi_{\rm gm}(r)$, so that

$$\Sigma(R) = 2\overline{\rho}\int_R^\infty \xi_{\rm gm}(r)\frac{r\,{\rm d}r}{\sqrt{r^2-R^2}}, \tag{3}$$

and

$$\Sigma(\leqslant R) = \frac{4\overline{\rho}}{R^2}\int_0^R y\,{\rm d}y\int_y^\infty \xi_{\rm gm}(r)\frac{r\,{\rm d}r}{\sqrt{r^2-y^2}} \tag{4}$$

with $\overline{\rho}$ the average background density of the Universe. Note in both equations, we have omitted the contribution from the mean density of the universe, as it does not contribute to the ESD. As we will see below, it is important to distinguish between the lensing signal due to host haloes (those haloes that are not embedded in a larger virialized structure) and subhaloes (haloes embedded in a host halo). In what follows we refer to galaxies at the centres of host- and subhaloes as central and satellite galaxies, respectively.

In the halo model, the dark matter distribution consists entirely of dark matter haloes, and the galaxy-mass cross-correlation function consists of four terms: three one-halo terms, and one two-halo term. The first one-halo term is due to the host haloes around central galaxies. Satellite galaxies contribute two one-halo terms: one describing the density distribution of the dark matter subhalo and one describing the density distribution of the host halo in which the subhalo is embedded. This latter term also depends on the relative location of the subhalo with respect to the centre of the parent halo. Finally, the two-halo term describes the correlation between the lens galaxy and the large-scale distribution of dark matter haloes. In this paper we focus only on the expected lensing signal at small R, and we will therefore ignore this two-halo term in what follows.

From the above, it is clear that central and satellite galaxies yield different lensing signals (see Hudson et al. 1998; Guzik & Seljak 2002; Yang et al. 2003a). In the past, various studies have used halo occupation statistics to model the total galaxy-mass cross-correlation function, due to central and satellite galaxies combined (Guzik & Seljak 2002; Mandelbaum et al. 2005b, 2006a; Yoo et al. 2005). Here, we adopt a different approach and we investigate the $\Delta\Sigma(R)$ of central and satellite galaxies separately. In Section 3 we show that with a decent galaxy group finder one can identify central and satellite galaxies, and probe their lensing signals separately.

2.1 Density distribution of haloes and subhaloes

As outlined above, the tangential shear due to galaxy–galaxy lensing can be used to infer the galaxy-mass cross-correlation function $\xi_{\rm gm}(r)$. On small scales, $\xi_{\rm gm}(r) = \rho(r)/\overline{\rho} - 1$, with $\rho(r)$ the azimuthally averaged density distribution around the lensing galaxies. This in turn reflects the density distribution of the host- and subhaloes surrounding central and satellite galaxies, respectively. For simplicity, we will not treat the baryonic masses of the lens galaxies as separate mass components, but instead consider them included in the halo components. As shown in Lin et al. (2006), the baryonic component can change the concentration of the total mass profile on small scales. We do not expect such effect to have an important impact on our results, because we are focusing on lensing signals on scales $R \gtrsim 50\ h^{-1}$ kpc.

For the host haloes, we adopt the following density profile:

$$\rho(r) = \frac{\rho_0}{(r/r_{\rm c})^\alpha(1+r/r_{\rm c})^{3-\alpha}}, \tag{5}$$

where

$$\rho_0 = \frac{\overline{\rho}\Delta_{\rm vir}}{3I(c,\alpha)}; \quad I(c,\alpha) \equiv \frac{1}{c^3}\int_0^c \frac{{\rm d}x}{x^{\alpha-2}(1+x)^{3-\alpha}} \tag{6}$$

(see e.g. Zhao 1996; Jing & Suto 2000). Note that $\alpha = 1$ corresponds to the NFW profile (Navarro, Frenk & White 1997); $\alpha = 1.5$ corresponds to the profile proposed by Moore et al. (1999) and $\alpha = 0$ corresponds to a density distribution with a constant density core. Although we will mainly focus on haloes with $\alpha = 1$, we also briefly discuss the impact of changing the central cusp slope. This is motivated by the fact that (i) observationally the exact value of the inner slope α is still uncertain (e.g. Swaters et al. 2003; Bartelmann & Meneghetti 2004; Gentile et al. 2004; Sand et al. 2004; Gentile et al. 2005; Meneghetti et al. 2005; Simon et al. 2005), (ii) numerical simulations suggest that haloes may reveal a fair amount of scatter in their central cusp slopes (e.g. Jing & Suto 2000; Dahle, Hannestad & Sommer-Larsen 2003; Power et al. 2003; Navarro et al. 2004) and (iii) the density distribution is interpreted as including the contribution from the baryons, so that it does not have to be in perfect accord with that of dark matter haloes.

For a given value of α, the density distribution of a dark matter host halo is specified by two parameters, a characteristic density ρ_0 and a characteristic radius $r_{\rm c}$. Alternatively, one can parametrize the

halo by its mass $M = (4\pi/3)\Delta_{\rm vir}\,\overline{\rho}\,r_{\rm vir}^3$ and concentration parameter $c = r_{\rm vir}/r_{\rm c}$. Here $r_{\rm vir}$ is the virial radius, defined so that the average density within it is $\Delta_{\rm vir}\overline{\rho}$. Throughout this paper we adopt $\Delta_{\rm vir} = 180$, and we use $M_{\rm h}$ and $M_{\rm s}$ to refer to the masses of host- and subhaloes, respectively.

Numerical simulations have shown that halo concentration is correlated with halo mass. Throughout we adopt the model of Eke, Navarro & Steinmetz (2001) to model the relation between c and M, and we assume that it is free of scatter. Therefore, the entire density distribution of a dark matter (host) halo is completely specified by its mass alone.

For subhaloes, we follow Hayashi et al. (2003), who, using numerical simulations, found that the density profiles of stripped dark matter subhaloes can be written as

$$\rho_{\rm s}(r) = \frac{f_{\rm t}}{1+(r/r_{\rm t,eff})^3}\,\rho(r). \tag{7}$$

Here $f_{\rm t}$ is a dimensionless measure for the reduction in central density, and $r_{\rm t,eff}$ is an 'effective' tidal radius that describes the outer cut-off imposed by tides. For $f_{\rm t} = 1$ and $r_{\rm t,eff} \gg r_{\rm c}$, equation (7) reduces to the original mass profile $\rho(r)$ given in equation (5), i.e. the mass profile before the subhalo was accreted by the host halo. The parameters $f_{\rm t}$ and $r_{\rm t,eff}$ are determined by the mass fraction of the subhalo that remains bound, $f_{\rm m}$. Fitting the mass profiles of numerous stripped dark matter subhaloes, Hayashi et al. (2003) obtained the following relations between $r_{\rm t,eff}$ (in units of the characteristic radius of the subhalo) and $f_{\rm m}$:

$$\log\left(\frac{r_{\rm t,eff}}{r_{\rm c}}\right) = 1.02 + 1.38\,\log f_{\rm m} + 0.37\,(\log f_{\rm m})^2, \tag{8}$$

and between $f_{\rm t}$ and $f_{\rm m}$:

$$\log f_{\rm t} = -0.007 + 0.35\log f_{\rm m} + 0.39(\log f_{\rm m})^2 + 0.23(\log f_{\rm m})^3. \tag{9}$$

Using a large cosmological numerical simulation, Gao et al. (2004) studied the radial dependence of the retained mass fraction $f_{\rm m}$ of a large sample of subhaloes. Using the results shown in their fig. 15, we obtain the following mean relation:

$$f_{\rm m} = 0.65\left(\frac{r_{\rm s}}{r_{\rm vir,h}}\right)^{2/3}, \tag{10}$$

where $r_{\rm s}$ is the distance of the subhalo from the centre of the host halo, and $r_{\rm vir,h}$ is the virial radius of the host halo. The combination of equations (7)–(10) gives a model for the density profile of a subhalo with a given original mass located at a given distance from its host halo.

Note that the above model for the density distribution of the host and subhaloes is only approximate. For example, host haloes of fixed mass show a fair amount of scatter in halo concentrations, correlated with the halo formation time (e.g. Wechsler et al. 2002; Zhao et al. 2003a,b; Lu et al. 2006), which we completely ignore. In addition, the retained mass fraction of subhaloes is assumed to depend only on the instantaneous location of the subhalo. In reality, however, subhaloes with the same $r_{\rm s}$ can have very different $f_{\rm m}$, depending on their orbital eccentricities and their time since being accreted by the host halo. Furthermore, equation (10) was obtained for host haloes with masses $\sim 10^{14}\,h^{-1}\,{\rm M}_\odot$, while we assume that it holds for haloes of all masses. Some of these shortcomings may affect our results. For example, as shown in Mandelbaum et al. (2005b), the scatter in the mass–luminosity relation can cause the derived mass to deviate from the mean sample halo mass, and so the uncertainty in the mass model of satellite galaxies may add uncertainty in our results. Unfortunately, a much more realistic model for the mass and density is not available at the present time, and we have to live with such uncertainties here.

2.2 Central galaxies

We first consider the lensing signal around central galaxies. At sufficiently small R we may simply replace $\overline{\rho}\xi_{\rm gm}(r)$ in equations (3) and (4) with the density distribution of the host halo, $\rho(r)$. In what follows, we use $\Delta\Sigma_{\rm c}(R)$ to refer to the ESD of central galaxies.

For NFW profiles (i.e. $\alpha = 1$) we can write (see Wright & Brainerd 2000),

$$\Delta\Sigma_{\rm c}(R) = \frac{M}{2\pi r_{\rm c}^2}\,I^{-1}(c,1)\left[g\left(\frac{R}{r_{\rm c}}\right) - f\left(\frac{R}{r_{\rm c}}\right)\right], \tag{11}$$

where

$$f(x) = \begin{cases} \frac{1}{x^2-1}\left[1 - \frac{\ln\left(\frac{1+\sqrt{1-x^2}}{x}\right)}{\sqrt{1-x^2}}\right] & \text{if } x < 1 \\ \frac{1}{3} & \text{if } x = 1 \\ \frac{1}{x^2-1}\left[1 - \frac{\operatorname{atan}\left(\sqrt{x^2-1}\right)}{\sqrt{x^2-1}}\right] & \text{if } x > 1 \end{cases} \tag{12}$$

and

$$g(x) = \begin{cases} \frac{2}{x^2}\left[\ln\left(\frac{x}{2}\right) + \frac{\ln\left(\frac{1+\sqrt{1-x^2}}{x}\right)}{\sqrt{1-x^2}}\right] & \text{if } x < 1 \\ 2 + 2\ln\left(\frac{1}{2}\right) & \text{if } x = 1 \\ \frac{2}{x^2}\left[\ln\left(\frac{x}{2}\right) + \frac{\operatorname{atan}\left(\sqrt{x^2-1}\right)}{\sqrt{x^2-1}}\right] & \text{if } x > 1. \end{cases} \tag{13}$$

As an illustration, Fig. 1 shows $\Delta\Sigma_{\rm c}$ as a function of the projected radius R for dark matter haloes with a mass $M_{\rm h} = 10^{13}\,h^{-1}\,{\rm M}_\odot$. The left-hand panel depicts cases in which the halo concentration is fixed at $c = 10$, but in which the inner cusp slope α changes from 0 to 2. The right-hand panel, on the other hand, shows results for NFW profiles ($\alpha = 1$) but with different concentrations. As expected, for a given c, a model with smaller α has a shallower ESD at small radii. For the model with a constant density core ($\alpha = 0$), the ESD goes to zero at the centre, because there is no central density gradient that can cause image distortions. For a given α, more concentrated haloes have a more concentrated ESD, as expected (see also Guzik & Seljak 2002). Comparing the results shown in the left- and right-hand panels, one can see that there is a degeneracy between the central density gradient and the concentration of a dark matter halo, at least for realistic observational errors in the tangential shear. A similar degeneracy also hampers a unique derivation of the density distribution of dark matter haloes from the rotation curves of disc galaxies (e.g. van den Bosch et al. 2000).

2.3 Satellite galaxies

The ESD around a satellite galaxy can be written as

$$\Delta\Sigma_{\rm s}(R|R_{\rm s}) = \Delta\Sigma_{\rm s,sub}(R) + \Delta\Sigma_{\rm s,host}(R|R_{\rm s}). \tag{14}$$

Here $\Delta\Sigma_{\rm s,sub}(R)$ and $\Delta\Sigma_{\rm s,host}(R\,|\,R_{\rm s})$ are the ESDs due to the dark matter subhalo and host halo, respectively, and $R_{\rm s}$ is the projected distance between the satellite galaxy and the centre of its host halo (throughout we assume that a satellite resides at the centre of its subhalo).

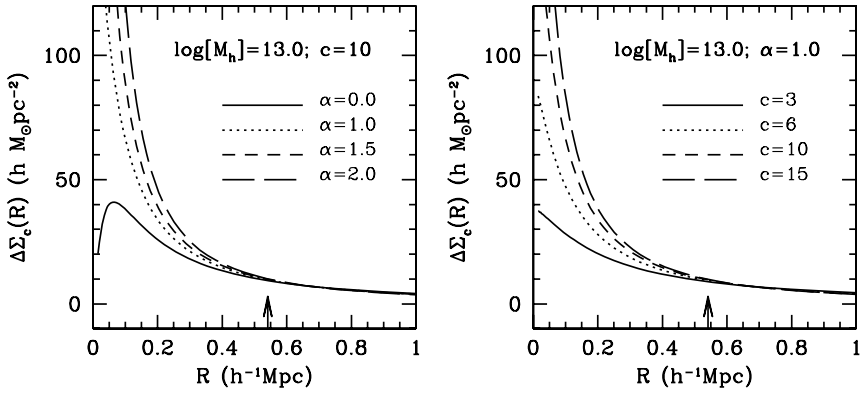

Figure 1. The ESD around central galaxies as a function of radius R. Results are shown for $10^{13}\,h^{-1}\,\mathrm{M}_\odot$ dark matter haloes with different density profiles. The left-hand panel shows model predictions for haloes with a concentration parameter $c = 10$ but with different values for the central cusp slope, α. The right-hand panel shows the ESDs of NFW profiles (i.e. $\alpha = 1$) with different concentration parameters, c. Note that in the presence of realistic measurement errors, there is a significant degeneracy between cusp slope and halo concentration. The arrows in both panels indicate the virial radius $r_{\rm vir}$ of a $10^{13}\,h^{-1}\,\mathrm{M}_\odot$ dark matter halo.

The azimuthally averaged, projected surface mass density of the host halo around a satellite galaxy located at a projected distance $R_{\rm s}$ from the halo centre is

$$\Sigma_{s,\rm host}(R\,;|\,;R_{\rm s}) = \frac{1}{2\pi}\int_0^{2\pi}\Sigma\left(\sqrt{R_{\rm s}^2+R^2+2R_{\rm s}R\cos\theta}\right)\mathrm{d}\theta, \quad (15)$$

where $\Sigma\,(R)$ is the projected density profile of the host halo. By integrating (15) from 0 to R one obtains $\Sigma_{s,\rm host}(\leqslant R\,|\,R_{\rm s})$, and thus the ESD $\Delta\Sigma_{s,\rm host}(R\,|\,R_{\rm s})$. The azimuthal averaging reflects the fact that in order to obtain sufficient signal-to-noise ratio to measure the tangential shear one has to stack many satellite galaxies with the same $R_{\rm s}$. As long as these have random orientation angles θ, the azimuthal averaging of equation (15) is appropriate.

To illustrate the ESD around satellite galaxies, we first show the contribution from the host halo, by assuming that the satellite galaxy has no corresponding subhalo [i.e. $\Sigma_{s,\rm sub}(R) = 0$]. Fig. 2 shows the model predictions of $\Delta\Sigma_{s,\rm host}(R\,|\,R_{\rm s})$ around satellite galaxies in NFW host haloes with masses of $10^{12}\,h^{-1}\,\mathrm{M}_\odot$ (left-hand panel) and $10^{14}\,h^{-1}\,\mathrm{M}_\odot$ (right-hand panel), respectively. Different line styles refer to different halo-centric distances, as indicated. For comparison, we also show the results for $R_{\rm s} = 0$ (solid lines), which are equivalent to the ESDs around central galaxies. Clearly, the ESD around satellite galaxies (without subhaloes) are very different from those around central galaxies. They start with a value close to zero at $R = 0$, decrease to a *negative* minimum near $R_{\rm s}$, and then increase rapidly with radius, eventually approaching the ESD of central galaxies at $R \gtrsim 3R_{\rm s}$. Note that here we are measuring the ESD $\Delta\Sigma_{\rm s,host}(R\,|\,R_{\rm s}) = \Sigma_{\rm s,host}(\leqslant R\,|\,R_{\rm s}) - \Sigma_{\rm s,host}(R\,|\,R_{\rm s})$ around satellite galaxies. When $\Sigma_{\rm s,host}(R\,|\,R_{\rm s})$ reaches its maximum value at around $R_{\rm s}$, the ESD decreases to its negative minimum. As expected, the overall amplitude of $\Delta\Sigma_{\rm s,host}(R\,|\,R_{\rm s})$ at large radii is higher for more massive haloes. Thus, if the value of $R_{\rm s}$ is known, the tangential shear $\gamma_{\rm t}(R)$ measured around satellite galaxies can be used to constrain the mass distribution of their host haloes. We will come back to this in Section 3.2.

We now include the contribution of the subhalo. For this, we use the subhalo model described in Section 2.1, which allows us to compute $\Delta\Sigma_{\rm s,sub}(R)$ for a given subhalo mass. This mass can be related to the subhalo mass at the time of accretion, using equation (10) and the true distance $r_{\rm s}$ of the subhalo from the centre of the host halo. In order to compute the contribution due to the host halo, $\Delta\Sigma_{\rm s,host}(R\,|\,R_{\rm s})$, one also needs to know $R_{\rm s}$, which is the projection of $r_{\rm s}$ on the plane of the sky (i.e. $0 \leqslant R_{\rm s} \leqslant r_{\rm s}$).

As an illustration, we consider a simple case in which all subhaloes have an original mass $M_{\rm s,0} = 10^{11.5}\,h^{-1}\,\mathrm{M}_\odot$ at the time of accretion. We model the tidal mass loss as described in

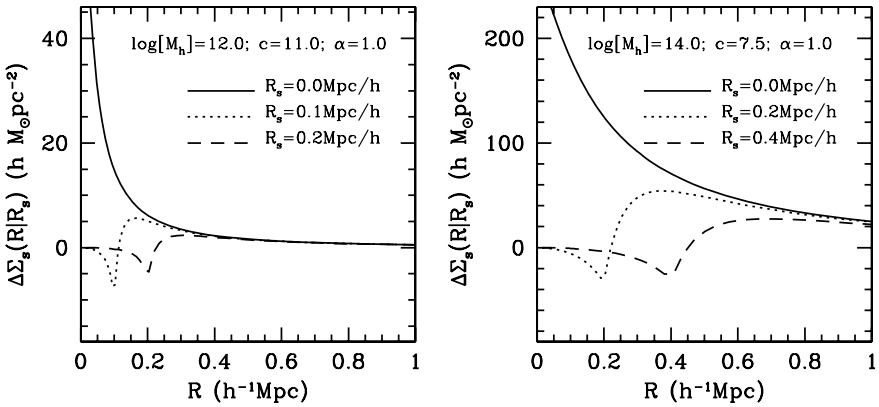

Figure 2. The ESD around central galaxies (solid lines) and satellite galaxies as a function of radius R. Here it is assumed that satellite galaxies are not associated with dark matter subhaloes; i.e. the ESD only reflects the contribution from the host halo. Different line styles correspond to different halo-centric distances of the satellite galaxies, as indicated. Panels of the left- and right-hand show the results for NFW host haloes with masses of 10^{12} and $10^{14}\,h^{-1}\,\mathrm{M}_\odot$, respectively.

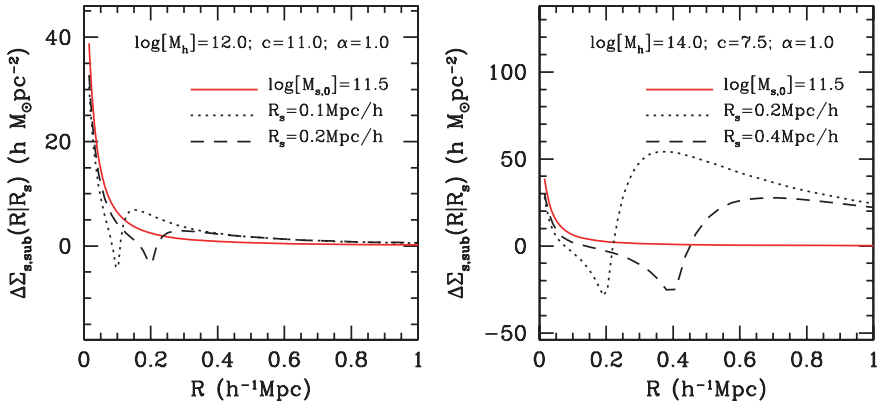

Figure 3. Same as Fig. 2, except that this time satellite galaxies are assumed to reside in subhaloes whose mass is equal to $M_{\rm s,0} = 10^{11.5}\,h^{-1}\,{\rm M}_\odot$ at the time of accretion. The solid lines correspond to the ESD of a halo of this mass with $R_{\rm s} = 0$, and are shown for comparison.

Section 2.1 and adjust their density profiles accordingly. Fig. 3 shows the full ESD (including both the host and the subhalo terms) around satellite galaxies located at different halo-centric distances in host haloes of different masses. For simplicity we assume that $R_{\rm s} = r_{\rm s}$, i.e. that the radius vector $\boldsymbol{r}_{\rm s}$ is perpendicular to the line of sight. Comparing Figs 3 and 2, one sees that the contribution of the subhalo to the ESD dominates at small R, as expected. As a comparison, the solid curves in Fig. 3 show the $\Delta\Sigma_{s,{\rm sub}}(R)$ of subhaloes with a mass $M_{\rm s} = 10^{11.5}\,h^{-1}\,{\rm M}_\odot$ (the contribution from the host term is ignored here). At small radii these are slightly higher than those represented by the dotted and dashed curves, because subhaloes are modelled to have lost a fraction $1 - f_{\rm m}$ of their mass after having been accreted by the host halo. Note that satellites with smaller $R_{\rm s}$ have a somewhat lower ESD at small radii. This owes to the fact that the mass loss is larger for subhaloes at a smaller halo-centric distance.

3 TEST USING GALAXIES AND GROUPS IN MOCK CATALOGUES

The analysis presented above shows that it is in principle possible to use galaxy–galaxy lensing to probe the mass distribution of haloes and subhaloes. Unfortunately, we do not know a priori whether a galaxy is a central galaxy or a satellite galaxy. Since the expected galaxy–galaxy lensing signal of individual galaxies is very weak, one has to combine the shear measured around a large number of galaxies to obtain a statistically significant detection. The ESD inferred from such a measurement is therefore the average over all lensing galaxies used. It is clear from the above, that if that average combines both central and satellite galaxies, the resulting $\Delta\Sigma(R)$ will be difficult to interpret, especially when the satellites have different $R_{\rm s}$.

However, if we could identify central and satellite galaxies a priori, and if we could also determine $R_{\rm s}$ for each satellite, we could measure the tangential shear of central and satellite galaxies separately, thus constraining the mean host halo mass as well as the mean subhalo mass of the satellites directly. Such an identification of central and satellite galaxies requires a method to decide which galaxies belong to the same dark matter halo. In a recent paper, Yang et al. (2005a) developed a new, halo-based group finder which is particularly successful in grouping galaxies in a redshift survey according to their common dark matter haloes. In this section, we apply this group finder to mock redshift catalogues and examine whether the membership information thus obtained is useful in galaxy–galaxy lensing studies. In particular, we examine whether the identification of central and satellite galaxies inferred from such a group catalogue is sufficiently reliable that it allows an accurate measurement of the masses of the corresponding host- and subhaloes.

3.1 *N*-body simulations and mock catalogues

We use the results of a high-resolution N-body simulation to construct mock galaxy catalogues. The simulation was carried out on the VPP5000 Fujitsu supercomputer of the National Astronomical Observatory of Japan with the vectorized-parallel P^{3}M code (Jing & Suto 2002). It evolves the distribution of the dark matter from an initial redshift of $z = 72$ down to 0 in a Λ cold dark matter (ΛCDM) 'concordance' cosmology with $\Omega_{\rm m} = 0.3$, $\Omega_\Lambda = 0.7$, $h = H_0/(100\,{\rm km\,s^{-1}\,Mpc^{-1}}) = 0.7$ and with a scale-invariant initial power spectrum with normalization $\sigma_8 = 0.9$. The simulation uses 512^3 cold dark matter particles in a periodic cube of $100 \times 100 \times 100\,h^{-3}$ Mpc^3. The particle mass is equal to $6.2 \times 10^8\,h^{-1}\,{\rm M}_\odot$, and dark matter haloes are identified using the standard FOF algorithm with a linking length of 0.2 times the mean inter-particle separation.

In order to construct realistic mock galaxy samples, we populate the haloes with galaxies, using the conditional luminosity function (hereafter CLF; Yang et al. 2003b; van den Bosch et al. 2003), $\Phi(L\,|\,M)$, which gives the average number of galaxies of luminosity L that reside in a halo of mass M. The CLF model parameters used to construct the mock galaxy catalogue are given in Table 1 of van den Bosch et al. (2005c) as ID # 6. We refer the reader to Yang et al. (2004) for details regarding the construction of these mock galaxy catalogues. We emphasize though, that by construction, these mock catalogues match the observed luminosity function and the observed clustering strength as a function of luminosity.

The CLF model allows us to populate each halo in the simulation with galaxies of different luminosities. We locate the brightest galaxy in each halo at the halo centre and assume that the other galaxies (the satellites) are associated with dark matter subhaloes. Unfortunately, we can not use the actual subhaloes in the numerical simulation itself, simply because the resolution of the simulation is not sufficient to resolve subhaloes in low mass host haloes. In addition, the survival and structure of subhaloes is affected by the baryonic component, which is not modelled in our dark matter only simulation. We therefore follow a different approach. We distribute the satellite galaxies isotropically throughout the host halo, with a

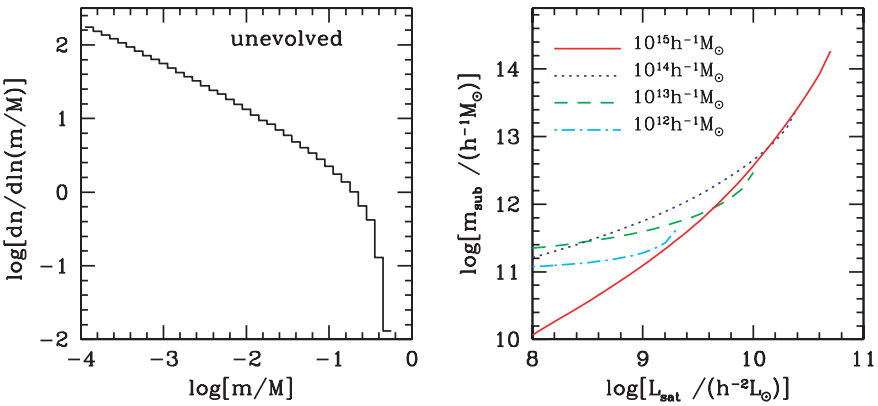

Figure 4. The left-hand panel shows the un-evolved mass function of dark matter subhaloes from van den Bosch et al. (2005a). Here 'un-evolved' means that the masses correspond to the masses of the subhaloes at the time that they were accreted (i.e. before any mass loss due to tidal stripping occurred). As shown in van den Bosch et al. (2005a), this mass function is independent of the mass of the host halo. The right-hand panel shows the relation between the luminosity of a satellite galaxy and the mass of the subhalo at the moment of accretion. This relation is obtained by comparing the number density of satellite galaxies predicted by the conditional luminosity function with the number density of subhaloes predicted by the un-evolved subhalo mass function shown in the left-hand panel.

number density distribution that reproduces the dark matter density profile. Note that here we use the spherical NFW profile with the concentration obtained by Eke et al. (2001) in modelling the spatial distribution of the satellite galaxies relative to the halo centre. Next, we model the subhalo population associated with these satellite galaxies adopting a prescription similar to that used in Kravtsov et al. (2004), Vale & Ostriker (2006) and Conroy et al. (2006): we assume that the luminosity of the satellite has a monotonic relation with the subhalo mass *at the time of its accretion*. In order to establish such a relation, we use the mass function of subhalo progenitors obtained by van den Bosch, Tormen & Giocoli (2005a), shown in the left-hand panel of Fig. 4, and the conditional luminosity function. The subhalo mass function has been studied recently both in numerical simulations and galaxy–galaxy lensing observations (e.g. De Lucia et al. 2004; Natarajan & Springel 2004; Natarajan et al. 2006). The mass–luminosity relations thus obtained are shown in the right-hand panel of Fig. 4, for four different host halo masses. Using these luminosity–mass relations and the model of subhalo structure described in Section 2.1, we assign each satellite a subhalo mass depending on (i) its luminosity, (ii) its host halo mass and (iii) its distance from the centre of the host halo.

Next we construct a mock redshift catalogue. We put the centre of the simulation box at a comoving distance of $200\,h^{-1}$ Mpc from a virtual observer. Each galaxy is given a redshift according to its distance from this observer and its peculiar velocity along the corresponding line of sight. We construct a flux-limited sample by including only those galaxies that have an apparent magnitude $m_{\rm bj} < 19.30$. Finally, we apply our halo-based group finder to this mock galaxy catalogue in order to construct a catalogue of galaxy groups. Following Yang et al. (2005b), we assign a halo mass to each group according to its ranking in total group luminosity and using the halo mass function for the standard ΛCDM cosmology (see Yang et al. 2005b, for more details). Tests in Yang et al. (2005b) and Weinmann et al. (2006) have shown that, on average, the group masses thus obtained are in good agreement with the input halo masses.

In what follows we refer to the brightest galaxy in each group as the central galaxy, and to all other group members as satellites. We use the mock galaxy group catalogue to test how well galaxy–galaxy lensing measurements around these 'central' and 'satellite' galaxies allow a recovery of their host and subhalo masses respectively. Due to interlopers (group members that do not belong to the same dark matter halo) and the fact that the group finder may occasionally miss a halo member, central and satellite galaxies in the group catalogue are not necessarily also central and satellite galaxies in their real haloes. If this confusion is too large, it will not be possible to obtain reliable estimates of host and/or subhalo masses. Clearly, the accuracy of such an approach therefore needs to be tested, which is the purpose of the mocks constructed here. In the left-hand panel of Fig. 5, we show the fractions of the false central galaxies and false satellite galaxies (interlopers) as a function of group mass. The fraction of false central galaxies is completely negligible in groups of all masses, while that of false satellites is typically well below 20 per cent. As we have pointed out in Section 2.3, the ESDs around satellite galaxies depend strongly on the projected halo-centric distances. Therefore, it is also important to check how the interloper fractions of the satellite galaxies depend on the projected group-centric distances. The results are shown in the right-hand panel of Fig. 5. One may note that at small projected group-centric distances the interloper fractions are rather small, and then increase (due to the larger area covered) as the projected group-centric distances increase. We will discuss later how and to what extent this interloper fraction may affect our measurements of the ESDs and the extracted properties of the subhaloes.

3.2 Lensing by galaxies in groups

3.2.1 The lensing signal around central galaxies

We first consider the lensing signal around the central group galaxies. In order to 'measure' the ESD we project the positions of galaxies and dark matter particles on to a plane perpendicular to the line of sight, and estimate the mean dark matter surface density contrast within rings of different radii around the galaxies. Since by definition the background surface density is subtracted, the ESD thus derived is independent of the depth of the projection (here equal to the simulation box size), as long as this depth is much larger than the dark matter correlation length.

The open circles in Fig. 6 show the $\Delta\Sigma(R)$ thus obtained around the central galaxies in groups with assigned masses in the range $12.0 \leqslant \log(M_{\rm h}/h^{-1}\,{\rm M}_\odot) < 12.5$ (left-hand panel) and $14.0 \leqslant \log(M_{\rm h}/h^{-1}\,{\rm M}_\odot) < 14.5$ (right-hand panel), respectively. These

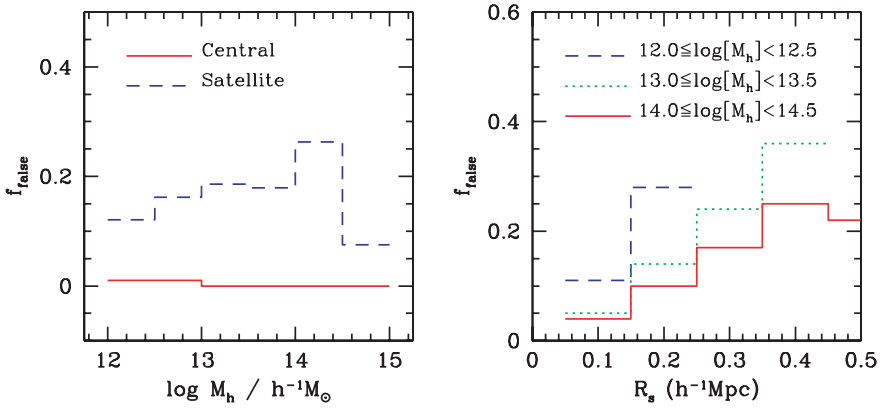

Figure 5. The left-hand panel shows the fractions of the false central (solid line) and satellite galaxies (dashed line) as a function of group masses. The right-hand panel shows the fractions of the false satellite galaxies (interlopers) in groups of different mass bins (as indicated) as a function of the projected group-centric distances.

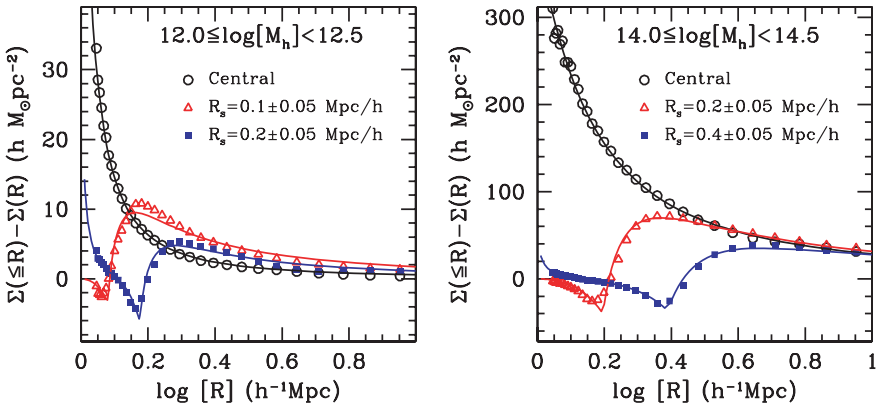

Figure 6. The ESDs measured from the *N*-body simulation around central galaxies (open circles) and around satellite galaxies at different R_s, as indicated (open triangles and solid squares) Note that here satellite galaxies are modelled without dark matter subhaloes. The two panels correspond to different bins of assigned group mass, as indicated with masses in h^{-1} $M_\odot$. The lines in each panel are the best-fitting models to the ESDs shown: for central galaxies, this model has two free parameter (M_h and c), while in the case of satellite galaxies it has four free parameters (M_h, c, M_s and R_s). Since we do not have realistic 'measurement' errors, we give each 'data point' equal weight in the fitting. See text for more details.

ESDs are monotonic functions of radius, and the amplitude is higher for the more massive haloes, in agreement with the predictions shown in Section 2. In Section 3.3, we investigate the accuracy with which these measurements allow a recovery of the mean host halo mass of these galaxies. Note that the group masses have been assigned based on the total group luminosity; the lensing signal will provide a direct test of this mass.

3.2.2 The lensing signal around satellite galaxies

As discussed in Section 2, the galaxy–galaxy lensing signal from satellite galaxies depends not only on the luminosity of the satellite, but also on the properties of the host halo and the halo-centric distance. This means that the tangential shear measured around a large sample of satellite galaxies in a given luminosity bin is very difficult to interpret. Rather, one can use the actual information from the group catalogue to sort the satellites according to both the mass of their host halo (i.e. the assigned group mass) and the projected distance from the centre of the group. Such a signal is much easier to interpret, as it tightly constrains the contribution of the $\Delta\Sigma_{s,\rm host}$-term to the shear measurements.

To illustrate the potential power of this approach we measure the ESD around satellite galaxies in our mock group catalogue, using the projected distribution of dark matter particles as in Section 3.2.1 above. Since the simulations do not resolve the majority of subhaloes, and since we did not associate satellite galaxies in the mock with the resolved subhaloes, this ESD reflects the lensing signal that one would obtain if satellite galaxies are not surrounded by dark matter subhaloes.

The open triangles and solid squares in Fig. 6 show the $\Delta\Sigma(R)$ around satellite galaxies with different projected distances from their central group galaxies, as indicated. As demonstrated in Section 2.3, the ESDs around satellite galaxies are expected to become similar to those around their central galaxies at radii $R \gtrsim 3R_s$. However, in Fig. 6 the ESDs of the satellite galaxies have slightly higher amplitudes at large radii than those of the corresponding central galaxies. This systematic offset is due to the fact that we have combined groups in a finite mass range. Since more massive haloes (groups) in general contain a larger number of satellite galaxies, any satellite-averaged mean, such as the ESD, will be biased towards the more massive haloes. A similar bias occurs when one tries to estimate the average halo mass of a stack of host galaxies from the

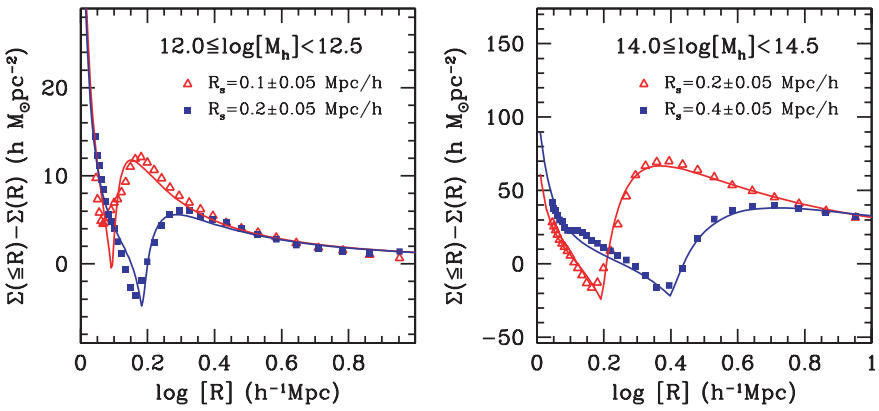

Figure 7. Same as Fig. 6, except that here satellite galaxies are associated with dark matter subhaloes, as described in the text. Note that this enhances the ESD at small R.

velocity dispersion of their satellite galaxies (see van den Bosch et al. 2004).

The ESD around satellite galaxies in groups with $10^{12} \leqslant M_{\rm h} < 10^{12.5}\,h^{-1}\,{\rm M}_{\odot}$ and with $R_{\rm s} = 0.2 \pm 0.05\,h^{-1}$ Mpc (solid squares in left-hand panel) reveals a small upturn at $R \lesssim 0.1\,h^{-1}$ Mpc. However, according to Fig. 2, $\Delta\Sigma(R)$ should go to zero at small R. This disagreement with the theoretical predictions is caused by the fact that a small number of these satellite galaxies in the group catalogue are interlopers, which in reality are mainly central galaxies in lower mass haloes. Since the interloper fraction increases with halo-centric distance (shown in the right-hand panel of Fig. 5), this explains why this peak near $R = 0$ is more pronounced for satellites with a larger $R_{\rm s}$. Clearly, it is important that any group finder used for identifying centrals and satellites is properly calibrated to yield sufficiently low interloper fractions. As described in Yang et al. (2005a), the group finder used here has been calibrated accordingly. In particular, the interloper fraction is constant (at ∼20 per cent) with group mass, unlike the more standard FOF method which typically yields an interloper fraction that increases systematically with decreasing group mass (see fig. 7 in Yang et al. 2005a).

We now add the contribution of the dark matter subhaloes. The density distribution of a subhalo surrounding a satellite galaxy of a given luminosity, located at a given halo-centric distance in a host halo of a given mass is modelled as described in Section 3.1, and its contribution to the lensing signal is computed by integrating $\rho_{\rm s}(r)$ along the line of sight. The resulting ESDs are shown in Fig. 7. As we have seen before, the contribution of the dark matter subhaloes enhances the ESD around satellite galaxies on small scales.

3.3 Estimating the masses of haloes and subhaloes from galaxy–galaxy lensing

Having estimated the lensing signal that one could in principle measure around central and satellite galaxies (given virtually infinite signal-to-noise ratio in the shear measurements), we now investigate to what extent such a signal allows to recover the average masses and concentration parameters of both the host haloes and the subhaloes.

3.3.1 The masses of haloes

We start by testing how accurately the lensing signal around galaxies classified as 'centrals' by our group finder allows a recovery of the mean mass and concentration of their host haloes. To that extent we use the assigned group masses as a 'pre-selection', and compute the $\Delta\Sigma_{\rm c}(R)$ around central galaxies in three group-mass bins, two of which are shown in Fig. 6. Assuming that the density distributions of dark matter haloes are well described by NFW profiles, we fit these $\Delta\Sigma_{\rm c}(R)$ using equation (11) with c and $M_{\rm h}$ as free parameters. The best fits are shown as solid lines in Fig. 6, and should be compared to the open circles.

The corresponding best-fitting values of $M_{\rm h}$ and c are shown in the left-hand panel of Fig. 8 as the open circles. For comparison, the asterisks show the true mean halo masses that host the mock galaxies used to determine $\Delta\Sigma_{\rm c}(R)$, while the hatched area indicates the bin of assigned group masses. Note that the best-fitting $M_{\rm h}$ is in good agreement with the true average, and that both lie well within the range of assigned group masses. The recovered concentration parameters also match the expected values predicted by Eke et al. (2001), indicated by the solid line, reasonably well. Although there are slight deviations, they are significantly smaller than the typical scatter in c for haloes of a given mass, $\Delta\log\ c \sim 0.14$, indicated by the error bars attached to the asterisks (e.g. Jing 2000; Bullock et al. 2001; Wechsler et al. 2002).

In the case of real galaxy–galaxy lensing data, the errors on $\Delta\Sigma_{\rm c}(R)$ will depend on the details of the selection of the lens-source samples and on the quality of the observational data. We do not model such errors here; instead we give each data point an equal weight in the fitting. We have also tested the impact of changing the weight scheme, the change in the best-fitting parameters is very small. Note that the error bars from recent galaxy–galaxy lensing measurements show different radial dependences (e.g. McKay et al. 2001; Mandelbaum et al. 2005a), the absence of realistic error bars on our 'measurements' prevents us from putting meaningful confidence levels on the best-fitting parameters.

The ESDs measured around satellite galaxies also contain information regarding the mass of the host halo. In order to see how well these lensing measurements allow to recover the masses of their host and subhaloes we fit with equation (14) the $\Delta\Sigma_{\rm s}(R \mid R_{\rm s})$ for a number of bins in $R_{\rm s}$. We have four free parameters in the fit: $M_{\rm h}$, c, $M_{\rm s}$ and $R_{\rm s}$ (subscripts 'h' and 's' refer to the host and subhaloes, respectively). Note that c is the concentration of the host halo, not that of the subhalo. Since the inner part of the ESDs cannot be measured with high precision, we assume that all subhaloes have a concentration $c_{\rm s} = 10$. We will discuss later in Section 3.3.2 how this assumption may affect the extracted properties (i.e. masses) of

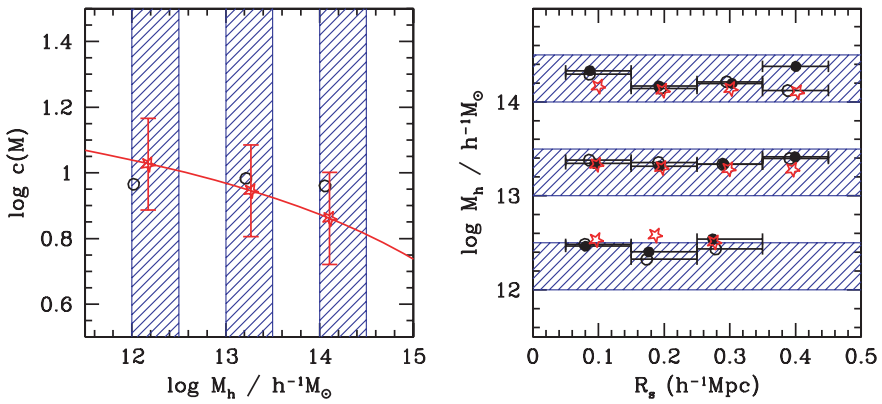

Figure 8. Properties of host haloes recovered from fitting the ESDs around central galaxies (left-hand panel) and satellite galaxies (right-hand panel) in the mock group catalogue. The hatched areas in both panels indicate the range of assigned masses of the groups from which the central and satellite galaxies are selected. The open circles in the left-hand panel indicate the masses and concentrations of the NFW haloes that best fit the ESDs of the central group galaxies. The asterisks show the true mean host halo masses and the corresponding halo concentrations obtained using the model of Eke et al. (2001; shown as solid line). The error bars on the asterisks correspond to $\Delta \log c = 0.14$ which reflects the typical scatter in c at a given halo mass. The solid dots and open circles in the right-hand panel indicate the best-fitting host halo masses and group-centric radii obtained from fitting the ESDs around satellite galaxies with and without subhalo contributions, respectively. The horizontal error bars on these points indicate the ranges of group-centric radius, R_s, that were used to select the satellite galaxies from the group catalogue. The asterisks indicate the true mean host halo masses and the true mean R_s, for the corresponding satellite galaxies.

the subhaloes. Note also that we let R_s be a free parameter, even though we only consider satellite galaxies in a relatively narrow bin in R_s (as determined from the group catalogue).

The best-fitting curves are given by the solid lines in Figs 6 and 7. Note that these best-fitting models are in reasonable agreement with the 'measured' ESD. The slight deviations are due to interlopers (i.e. errors associated with the group catalogue) and to the fact that the model does not account for the fact that the data corresponds to a range in host and subhalo masses (i.e. $\Delta\Sigma_s(R \mid R_s)$ reflects a linear combination of many slightly different ESDs). The best-fitting host halo masses are shown in the right-hand panel of Fig. 8: solid dots are the results obtained using the mock in which we do not include the analytical subhaloes (Fig. 6), while the open circles show the results obtained when subhaloes are included (Fig. 7). The agreement with the true mean host halo masses, indicated by the asterisks, is extremely good, suggesting that the lensing signal from satellite galaxies basically yields an equally good measurement of the host halo mass as that from the central galaxies. Thus, with a well-defined group catalogue, the properties of the host haloes can be accurately recovered from the ESDs using both central and satellite galaxies.

There is one small caveat though. Note that the host halo masses obtained from the central galaxies are somewhat lower than those obtained from the satellites. This is again due to the fact that the ESDs of satellite galaxies are weighted by the number of satellite galaxies; since there are more satellite galaxies in more massive groups, more massive systems receive a larger weight in the averaging. In particular, groups that consist only of a single member (which then by definition is a central galaxy), only contribute to $\Delta\Sigma_c$, but not to $\Delta\Sigma_s$. Since such a group is likely to have a relatively low mass compared to the other groups in the same mass bin, this will bias the value of M_h inferred from the satellites high with respect to the value of M_h inferred from the central galaxies. Note, however, that this does not reflect an error; the average true halo mass of systems with at least one satellite is simply larger than the average true halo mass of all systems (including those with zero satellites). This is also evident from the fact that the asterisks in the left- and right-hand panels of Fig. 8 indicate different masses. Thus, if the host masses inferred from $\Delta\Sigma_c$ and $\Delta\Sigma_s$ do not agree with each other, this does not necessarily indicate an inconsistency. It may also simply reflect a 'selection effect', in that the ESDs around central and satellite galaxies are contributed by somewhat different host halo populations. As a simple test, we weight the ESDs for central galaxies with the number of satellite galaxies at different group-centric distances. The recovered host halo masses are now in much better consistent with those recovered from the ESDs around satellite galaxies.

3.3.2 The masses of subhaloes

The four-parameter fits to the ESDs of satellite galaxies also yield best-fitting values for the average subhalo mass, M_s and for the projected distance, R_s. The open circles in Fig. 9 show the best-fitting values of M_s and R_s as obtained from the mock in which we added analytical subhaloes around each satellite galaxy (i.e. these correspond to the ESDs shown in Fig. 7). For comparison, the asterisks show the corresponding true mean values.[1] The solid squares in Fig. 9 indicate the best-fitting values of M_s obtained from the mock in which no subhaloes are included (i.e. corresponding to the ESDs shown in Fig. 6). The fact that these best-fitting values are not equal to zero, as they should be, owes to the presence of interlopers that in reality are centrals. These best-fitting subhalo masses should therefore be considered a contamination of the measurement in the case *with* subhaloes. Typically this contamination is much smaller than the actual mean subhalo mass, especially at small R_s. In the cases examined here, the largest contamination we find is for the satellites with $R_s = 0.3 \pm 0.05\,h^{-1}$ Mpc in groups with $10^{12} \leqslant M_h < 10^{12.5}\,h^{-1}\,M_\odot$, where the best-fitting M_s inferred from the mock without subhaloes is 38 per cent of that obtained with subhaloes. In all other cases this fraction is much lower.

The shaded areas in Fig. 9 outline the 90-percentile range of the real subhalo masses, which clearly is very broad. This owes to the

[1] For interlopers that are centrals, rather than satellites, we use the host halo mass in the computation of the averages.

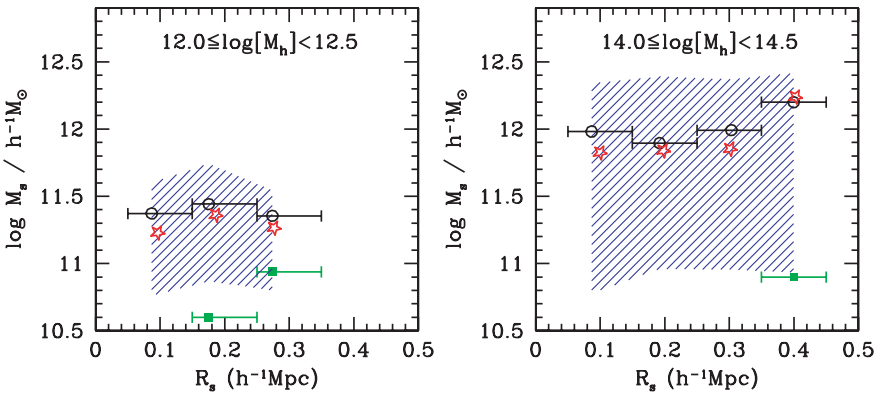

Figure 9. Open circles indicate the best-fitting subhalo masses and group-centric radii obtained from fitting the ESDs around satellite galaxies in the mock group catalogue in which each satellite galaxy has been assigned a dark matter subhalo as described in Section 3. Different panels correspond to groups in different bins of assigned mass, as indicated, while the horizontal error bars indicate the ranges of R_s that were used to select the satellite galaxies from the group catalogue. The hatched areas show the 90 percentile ranges of true (retained) subhalo masses. The asterisks indicate the true mean subhalo masses and the true mean R_s, for the corresponding satellite galaxies. Finally, the solid squares (also with horizontal error bars) indicate the best-fitting values of M_s and R_s obtained by fitting the ESDs around the satellite galaxies in the mock *without* dark matter subhaloes. The fact that these best-fitting values are not equal to zero, as they should be, owes to the contamination due to interlopers. See text for a detailed discussion.

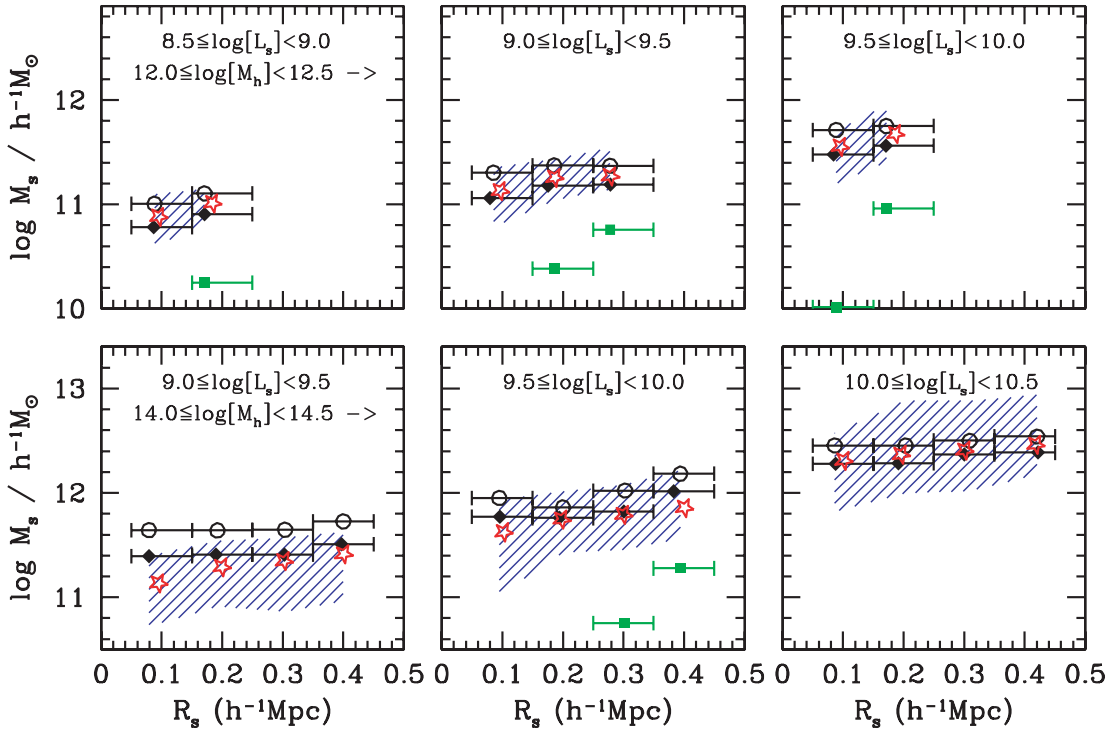

Figure 10. Same as Fig. 9, except that here we show the results for different bins in satellite luminosity L_s, as indicated in $h^{-2}\,L_\odot$. As in Fig. 9 the open circles show the best-fitting subhalo masses and group-centric radii obtained fitting the ESDs assuming NFW subhaloes with $c_s = 10$. The solid diamonds show the same quantities but obtained by assuming subhaloes modelled by equation (7) with mean $\langle r_s \rangle \approx (R_s + r_{\rm vir,h})/2$.

fact that we have added the lensing signal from all satellite galaxies, irrespective of their luminosity. In our model, and most likely also in reality, more luminous satellites reside in more massive subhaloes. This suggests that the actual range of subhaloes probes may be narrowed by selecting satellite galaxies of similar luminosities. Fig. 10 shows the ESDs around satellite galaxies in different luminosity bins and in groups of different (assigned) masses. As in Fig. 9, the shaded areas indicate the 90-percentile ranges of the true subhalo masses. As expected, these are now much narrower. The remaining width owes to the finite widths of the ranges in satellite luminosity, L_s, group mass, M_h, and projected separation, R_s, and to the fact that projection causes systems with different r_s to contribute to the same R_s. Note that in our model the subhalo mass is a function of M_h, L_s and r_s.

The open circles in Fig. 10 indicate the best-fitting subhalo masses, obtained by fitting the corresponding ESDs with a four-parameter model as described above. Note that the recovered subhalo masses are slightly larger than the input value, especially for fainter satellite galaxies in massive groups. We propose that the main reason for this is that a stripped halo has a steeper mass profile

(see equation 7), and the assumption of a fixed NFW profile with $c_s = 10$ is not sufficiently accurate. As a simple test of this hypothesis, we consider a simple model in which we assume that the mean halo-centric distances of the satellite galaxies in each sample is $\langle r_s \rangle \approx (R_s + r_{vir,h})/2$. Then, we use equation (7) to model the mean profile of the subhaloes in consideration. This model ensures that subhaloes with smaller R_s, which are expected to have suffered more mass loss, are more concentrated. The best-fitting subhalo masses obtained from this model are shown in Fig. 10 as the solid diamonds. As can be seen, the best-fitting masses are systematically smaller than in the case of $c_s = 10$, and are in better agreement with the true averages.

In conclusion, with a well-defined group catalogue, the ESDs of satellite galaxies obtained from galaxy–galaxy lensing, with signals properly stacked according to the group masses (inferred from the total group luminosities) and the luminosities and group-centric distances of satellite galaxies, can be used to probe the masses of subhaloes associated with satellite galaxies.

3.3.3 What if the brightest galaxy is off-centre?

In the analysis presented above, the brightest halo galaxy is assumed to reside at the halo centre. In reality, the location of the brightest galaxy may not be exactly at the halo centre, and this may affect the predicted ESDs around the central and satellite galaxies. Here, we examine the importance of this effect.

In a recent study of the phase-space distribution of the brightest halo galaxies in galaxy groups, van den Bosch et al. (2005b) found that, for haloes with masses $M_h > 10^{13} h^{-1} M_\odot$, the deviation of the location of the brightest galaxy from the halo centre is about 3 per cent of the halo virial radius. Based on SPH simulations, Berlind et al. (2003) also found that the 'central' galaxy in a dark matter halo may deviate from the position of the most bound particle by 2 per cent of the halo virial radius. In order to quantify how such deviations impact on the ESDs, we perform the following test. We construct a new mock catalogue in which we assume that the position of each brightest halo galaxy deviates from the most bound particle with an amount given by a Gaussian distribution with a dispersion equal to 3 per cent of the halo virial radius. Next we run our group finder over this new mock catalogue, compute the ESDs around the central and satellites galaxies, and fit them as described above to determine the best-fitting halo masses and concentrations. We find that the off-centring of the central galaxies has an almost negligible effect, except that the best-fitting concentration parameters of host haloes are reduced by a modest 15 per cent. Such a reduction arises from the fact that the off-centring decreases the ESD at small radius, similar to what happens to the ESD around satellite galaxies. Thus, the ability to measure the host halo masses is not compromised by the fact that central galaxies may be (slightly) off-centred from the gravitational centre of their dark matter halo.

4 DISCUSSION AND CONCLUSIONS

The weak galaxy–galaxy lensing signals from central and satellite galaxies (at different halo-centric distances) are very different. So far, this difference has not been fully exploited. In fact, in all previous studies it has been considered a nuisance, rather than a source of valuable information. Most galaxy–galaxy lensing analyses either have simply ignored the differences between central and satellite galaxies, or have focused on isolated galaxies in an attempt to minimize the disturbing contribution of satellite galaxies. An alternative approach, pioneered by Guzik & Seljak (2002), is to model the combined lensing signal from central and satellites. However, no study to date has attempted to measure the lensing signals of centrals and satellites at different halo-centric distances separately. This simply owes to the fact that it is not a priori clear which galaxy is a central galaxy and which galaxy a satellite. This is unfortunate, as a separation of these two components would allow a much cleaner measurement of the halo masses (and their detailed density profiles) hosting central galaxies. In addition, it would allow for a direct measurement of the masses (and density profiles) of subhaloes hosting satellite galaxies. Furthermore, since the shear around satellite galaxies also harbours information regarding the host haloes in which their subhaloes reside, one can use their lensing signal to obtain an independent measurement of the host halo masses.

In order to exploit this richness in information, it is crucial that one has a reliable technique for separating central and satellite galaxies. In this paper, we have investigated to what extent this is feasible with the halo-based group finder developed by Yang et al. (2005a). This group finder is straightforward to apply to galaxy redshift surveys, and has been calibrated to yield low interloper fractions. The latter is important to minimize the confusion of centrals and satellites. In order to test our methodology, we constructed detailed mock redshift surveys from *N*-body simulations that are populated with galaxies using the conditional luminosity function. Application of the halo-based group finder to this mock redshift survey yields a large catalogue of mock galaxy groups, from which central galaxies are identified as the brightest galaxy in each group. All other group members are considered to be satellites.

The group catalogue is not only useful to separate centrals from satellites. It also yields, for each satellite, the projected separation, R_s, to it central galaxy. This is extremely important, since the contribution of the host halo to the gravitational shear around a satellite galaxy depends strongly on R_s. Therefore, in order to facilitate a meaningful interpretation of the shear measurements around satellite galaxies, it is crucial that one only stacks the data from a relatively narrow bin in R_s. Another piece of useful information from the group finder are the masses that one can assign to each group based on the total luminosity of all its members. This mass can be used to 'pre-select' central and satellite galaxies in relatively narrow bins in the group mass, which again facilitates the interpretation of the lensing measurements.

To test these ideas we computed the ESD, which is the observable that can be obtained from the lensing measurements, around each central and satellite galaxy in the *N*-body simulation. We have demonstrated that by stacking the ESDs around central galaxies within different group mass bins, the average masses and concentrations of their host haloes can be accurately recovered from the data. In addition, we have shown that the ESDs around satellite galaxies, when stacked according to group-centric distance and group mass, allow an equally accurate recovery of the masses of their corresponding subhaloes, as well as that of their host haloes.

We therefore conclude that a combination of galaxy-galaxy lensing measurements with a galaxy group catalogue extracted from a large-redshift survey, such as the SDSS, in principle allows for accurate measurements of the masses and concentrations of host haloes around central galaxies and subhaloes around satellite galaxies. However, it is important to realize that we have not attempted to mimic realistic observations. Rather, we have simply assumed infinite accuracy in the measurements of the ESDs. In reality, resolution issues, due to the finite sampling of the shear field and errors in the shear measurements, may cause a substantial reduction of the accuracy with which this methodology can be applied. In a forthcoming paper, we will apply this method to realistic mock shear

maps taking into account various observational effects to test its feasibility.

ACKNOWLEDGMENTS

We thank Michael Hudson for useful comments. XY is supported by the *One Hundred Talents* project of the Chinese Academy of Sciences and grants from NSFC (Nos.10533030, 10673023). YPJ is supported by the grants from NSFC (Nos. 10125314, 10373012, 10533030) and from Shanghai Key Projects in Basic research (No. 04JC14079 and 05XD14019).

REFERENCES

Bartelmann M., Meneghetti M., 2004, A&A, 418, 413
Bartelmann M., 1996, A&A, 313, 697
Benson A. J., Lacey C. G., Baugh C. M., Cole S., Frenk C. S., 2002, MNRAS, 333, 156
Berlind A. A., Weinberg D. H., 2002, ApJ, 575, 587
Berlind A. A. et al., 2003, ApJ, 593, 1
Brainerd T. G., Specian M. A., 2003, ApJ, 593, L7
Brainerd T. G., Blandford R. D., Smail I., 1996, ApJ, 466, 623
Bullock J. S., Kolatt T. S., Sigad Y., Somerville R. S., Kravtsov A. V., Klypin A. A., Primack J. R., Dekel A., 2001, MNRAS, 321, 559
Cole S., Lacey C. G., Baugh C. M., Frenk C. S., 2000, MNRAS, 319, 168
Conroy C. et al., 2005, ApJ, 635, 982
Conroy C., Wechsler R. H., Kravtsov A. V., 2006, ApJ, 647, 201
Cooray A., 2005, MNRAS, 364, 303
Cooray A., 2006, MNRAS, 365, 842
Croton D. J. et al., 2006, MNRAS, 365, 11
Dahle H., Hannestad S., Sommer-Larsen J., 2003, ApJ, 588, 73
dell'Antonio I. P., Tyson J. A., 1996, ApJ, 473, L17
De Lucia G., Kauffmann G., Springel V., White S. D. M., Lanzoni B., Stoehr F., Tormen G., Yoshida N., 2004, MNRAS, 348, 333
Eke V. R., Navarro J. F., Steinmetz M., 2001, ApJ, 554, 114
Fischer P. et al., 2000, AJ, 120, 1198
Fardal M. A., Katz N., Gardner J. P., Hernquist L., Weinberg D. H., Dav'e R., 2001, ApJ, 562, 605
Gao L., White S. D. M., Jenkins A., Stoehr F., Springel V., 2004, MNRAS, 355, 819
Gentile G., Salucci P., Klein U., Vergani D., Kalberla P., 2004, MNRAS, 351, 903
Gentile G., Burkert A., Salucci P., Klein U., Walter F., 2005, ApJ, 634L, 145
Griffiths R. E., Casertano S., Im M., Ratnatunga K. U., 1996, MNRAS, 282, 1159
Guzik J., Seljak U., 2001, MNRAS, 321, 439
Guzik J., Seljak U., 2002, MNRAS, 335, 311
Hayashi E., Navarro J. F., Taylor J. E., Stadel J., Quinn T., 2003, ApJ, 584, 541
Hoekstra H., Franx M., Kuijken K., Carlberg R. G., Yee H. K. C., 2003, MNRAS, 340, 609
Hoekstra H., Yee H. K. C., Gladders M. D., 2004, ApJ, 606, 67
Hoekstra H., Hsieh B. C., Yee H. K. C., Lin H., Gladders M. D., 2005, ApJ, 635, 73
Hudson M. J., Gwyn S. D. J., Dahle H., Kaiser N., 1998, ApJ, 503, 531
Jing Y. P., 2000, ApJ, 535, 30
Jing Y. P., Suto Y., 2000, ApJ, 529L, 69
Jing Y. P., Suto Y., 2002, ApJ, 574, 538
Jing Y. P., Mo H. J., Börner G., 1998, ApJ, 494, 1
Kang X., Jing Y. P., Mo H. J., Börner G., 2005, ApJ, 631, 21
Kauffmann G., White S. D. M., Guiderdoni B., 1993, MNRAS, 264, 201
Kauffmann G., White S. D. M., Heckman T. M., Menard B., Brinchmann J., Charlot S., Tremonti C., Brinkmann J., 2004, MNRAS, 353, 713
Katz N., Weinberg D. H., Hernquist L., 1996, ApJS, 105, 19
Kay S. T., Pearce F. R., Frenk C. S., Jenkins A., 2002, MNRAS, 330, 113
Kleinheinrich M. et al., 2006, A&A, 455, 441
Kravtsov A. V., Berlind A. A., Wechsler R. H., Klypin A. A., Gottlöber S., Allgood B., Primack J. R., 2004, ApJ, 609, 35
Klypin A., Kravtsov A. V., Bullock J. S., Primack J. R., 2001, ApJ, 554, 903
Lu Y., Mo H. J., Katz N., Weinberg M. D., 2006, MNRAS, 368, 1931
Lin W. P., Jing Y. P., Mao S., Gao L., McCarthy I. G., 2006, preprint (astro-ph/0607555)
McKay T. A. et al., 2001, preprint (astro-ph/0108013)
McKay T. A. et al., 2002, ApJ, 571, L85
Mandelbaum R. et al., 2005a, MNRAS, 361, 1287
Mandelbaum R., Tasitsiomi A., Seljak U., Kravtsov A., Wechsler R. H., 2005b, MNRAS, 362, 1451
Mandelbaum R., Seljak U., Kauffmann G., Hirata C. M., Brinkmann J., 2006a, MNRAS, 368, 715
Mandelbaum R., Seljak U., Cool R. J., Blanton M., Hirata C. M., Brinkmann J., 2006b, preprint (astro-ph/0605476)
Meneghetti M., Bartelmann M., Jenkins A., Frenk C., 2005, preprint (astro-ph/0509323)
Miralda-Escudé J., 1991, ApJ, 370, 1
Mo H. J., Fukugita M., 1996, ApJ, 467, L9
Mo H. J., Mao S., White S. D. M., 1998, MNRAS, 295, 319
Moore B., Quinn T., Governato F., Stadel J., Lake G., 1999, MNRAS, 310, 1147
Natarajan P., Kneib J. P., 1997, MNRAS, 287, 833
Natarajan P., Springel V., 2004, ApJ, 617L, 13
Natarajan P., De Lucia G., Springel V., 2006, preprint (astro-ph/0604414)
Navarro J. F., Frenk C. S., White S. D. M., 1997, ApJ, 490, 493
Navarro J. F. et al., 2004, MNRAS, 349, 1039
Parker L. C., Hudson M. J., Carlberg R. G., Hoekstra H., 2005, ApJ, 634, 806
Prada F. et al., 2003, ApJ, 598, 260
Power C., Navarro J. F., Jenkins A., Frenk C. S., White S. D. M., Springel V., Stadel J., Quinn T., 2003, MNRAS, 338, 14
Reed D., Governato F., Quinn T., Gardner J., Stadel J., Lake G., 2005, MNRAS, 359, 1537
Sand D. J., Treu T., Smith G. P., Ellis R. S., 2004, ApJ, 604, 88
Schneider P., 2005, in Meylan G., Jetzer P., North P., Kochanek C. S., Schneider P., Wambsganss J., eds, Gravitational Lensing: Strong, Weak & Micro. Springer-Verlag, Berlin, p. 273
Seljak U., 2000, MNRAS, 318, 203
Sheldon E. S. et al., 2004, AJ, 127, 2544
Simon J. D., Bolatto A. D., Leroy A., Blitz L., Gates E. L., 2005, ApJ, 621, 757
Smith D. R., Bernstein G. M., Fischer P., Jarvis M., 2001, ApJ, 551, 643
Somerville R. S., Primack J. R., 1999, MNRAS, 310, 1087
Spergel D. N. et al., 2006, preprint (astro-ph/0603449)
Springel V., 2005, MNRAS, 364, 1105
Springel V. et al., 2005, Nat, 435, 629
Swaters R., Madore B. F., van den Bosch F. C., Balcells M., 2003, ApJ, 583, 732
Tasitsiomi A., Kravtsov A. V., Wechsler R. H., Primack J. R., 2004, ApJ, 614, 533
Tinker J. L., Weinberg D. H., Zheng Z., Zehavi I., 2005, ApJ, 631, 41
Tyson J. A., Valdes F., Jarvis J. F., Mills A. P., Jr., 1984, ApJ, 281L, 59
Vale A., Ostriker J. P., 2004, MNRAS, 353, 189
Vale A., Ostriker J. P., 2006, MNRAS, 371, 1173
van den Bosch F. C., 2002, MNRAS, 332, 456
van den Bosch F. C., Robertson B. E., Dalcanton J. J., de Blok W. J. G., 2000, AJ, 119, 1579
van den Bosch F. C., Yang X., Mo H. J., 2003, MNRAS, 340, 771
van den Bosch F. C., Norberg P., Mo H. J., Yang X., 2004, MNRAS, 352, 1302
van den Bosch F. C., Tormen G., Giocoli C., 2005a, MNRAS, 359, 1029
van den Bosch F. C., Weinmann S. M., Yang X., Mo H. J., Li C., Jing Y. P., 2005b, MNRAS, 351, 1203
van den Bosch F. C., Yang X., Mo H. J., Norberg P., 2005c, MNRAS, 356, 1233
Wechsler R. H., Bullock J. S., Primack J. R., Kravtsov A. V., Dekel A., 2002, ApJ, 568, 52

Weinberg D. H., Dav'e R., Katz N., Hernquist L., 2004, ApJ, 601, 1
Weinmann S. M., van den Bosch F. C., Yang X., Mo H. J., 2006, MNRAS, 366, 2
White M., 2001, MNRAS, 321, 1
White S. D. M., Frenk C., 1991, ApJ, 379, 52
Wilson G., Kaiser N., Luppino G. A., Cowie L. L., 2001, ApJ, 555, 572
Wright C. O., Brainerd T. G., 2000, ApJ, 534, 34
Yang X., Mo H. J., Kauffmann G., Chu Y. Q., 2003a, MNRAS, 339, 387
Yang X., Mo H. J., van den Bosch F. C., 2003b, MNRAS, 339, 1057
Yang X., Mo H. J., Jing Y. P., van den Bosch F. C., Chu Y., 2004, MNRAS, 350, 1153
Yang X., Mo H. J., van den Bosch F. C., Jing Y. P., 2005a, MNRAS, 356, 1293
Yang X., Mo H. J., Jing Y. P., van den Bosch F. C., 2005b, MNRAS, 358, 217
Yoo J., Tinker J. L., Weinberg D. H., Zheng Z., Katz N., Davé R., 2005, ApJ, in press (astro-ph/0511580)
Zaritsky D., White S. D. M.,, 1994, ApJ, 435, 599
Zhao D. H., Mo H. J., Jing Y. P., Börner G., 2003a, MNRAS, 339, 12
Zhao D. H., Jing Y. P., Mo H. J., Börner G., 2003b, ApJ, 597L, 227
Zhao H., 1996, MNRAS, 278, 488
Zheng Z. et al., 2005, ApJ, 633, 791

This paper has been typeset from a TEX/LATEX file prepared by the author.